AFRL-AFOSR-VA-TR-2024-0034

Topological photonics for enabling high-power lasers

Soljacic, Marin
MASSACHUSETTS INSTITUTE OF TECHNOLOGY
77 MASSACHUSETTS AVE
CAMBRIDGE, MA, 02139
USA

11/22/2023
Final Technical Report

Air Force Research Laboratory
Air Force Office of Scientific Research
Arlington, Virginia 22203
Air Force Materiel Command

REPORT DOCUMENTATION PAGE

PLEASE DO NOT RETURN YOUR FORM TO THE ABOVE ORGANIZATION.

1. REPORT DATE	2. REPORT TYPE	3. DATES COVERED	
20231122	Final	START DATE 20200615	END DATE 20230614

4. TITLE AND SUBTITLE
Topological photonics for enabling high-power lasers

5a. CONTRACT NUMBER	5b. GRANT NUMBER	5c. PROGRAM ELEMENT NUMBER
	FA9550-20-1-0115	61102F
5d. PROJECT NUMBER	**5e. TASK NUMBER**	**5f. WORK UNIT NUMBER**

6. AUTHOR(S)
Marin Soljacic

7. PERFORMING ORGANIZATION NAME(S) AND ADDRESS(ES)
MASSACHUSETTS INSTITUTE OF TECHNOLOGY
77 MASSACHUSETTS AVE
CAMBRIDGE, MA 02139
USA

8. PERFORMING ORGANIZATION REPORT NUMBER

9. SPONSORING/MONITORING AGENCY NAME(S) AND ADDRESS(ES)	10. SPONSOR/MONITOR'S ACRONYM(S)	11. SPONSOR/MONITOR'S REPORT NUMBER(S)
Air Force Office of Scientific Research 875 N. Randolph St. Room 3112 Arlington, VA 22203	AFRL/AFOSR RTB1	AFRL-AFOSR-VA-TR-2024-0034

12. DISTRIBUTION/AVAILABILITY STATEMENT
A Distribution Unlimited: PB Public Release

13. SUPPLEMENTARY NOTES

14. ABSTRACT
In this project, we focus on developing topological photonics for enabling high?power lasers. To further this objective, theoretical research was conducted that spans a variety of domains. In one body of work, we used machine learning and mathematical tools to describe the topological nature of photonic crystals, with a goal of finding new topological photonic crystals to enable lasers. In another body of work, we developed novel concepts for lasers based on nonlinear gain and loss mechanisms, which can be used to generate quantum states of light far below the shot noise limit. Such lasers rely on dispersion and interference mechanisms that could one day be implemented through topological means. In a final body of work, we developed a theoretical formalism for describing the optical properties of time?dependent materials, and showed how these materials can be used as novel gain sources for potential lasers.

15. SUBJECT TERMS

16. SECURITY CLASSIFICATION OF:			17. LIMITATION OF ABSTRACT	18. NUMBER OF PAGES
a. REPORT	b. ABSTRACT	c. THIS PAGE		
U	U	U	UU	19

19a. NAME OF RESPONSIBLE PERSON	19b. PHONE NUMBER *(Include area code)*
JOHN LUGINSLAND	000-0000

Standard Form 298 (Rev.5/2020)
Prescribed by ANSI Std. Z39.18

Annual Report for Grant FA9550-20-1-0115 (Sept 2023)
Topological photonics for enabling high-power lasers

List of Sections:

1 - Automated Discovery and Optimization of 3D Topological Photonic Crystals

2 - Location and topology of the fundamental gap in photonic crystals

3 - Generating macroscopic intensity noise-squeezed states of light in semiconductor lasers

4 - Intense squeezed light from lasers with sharply nonlinear gain

5 - Optical properties of dispersive time-dependent materials

Published Content

Annual Report for Grant FA9550-20-1-0115 (Sept 2023)
Topological photonics for enabling high-power lasers

Automated Discovery and Optimization of 3D Topological Photonic Crystals

The past few decades have seen tremendous advances in optimization and inverse design techniques for nanophotonic components and, in particular, photonic crystals (PhCs). In particular, topological PhCs have received considerable attention for their promised robustness for photonic devices and their ability to manipulate and guide light in unique ways [1-3]. In contrast to their electronic counterparts, topological PhCs offer the exciting prospect of a flexible and tunable design space, with structural morphology subject only to the limits of fabrication constraints. This design freedom has not only endowed photonics with the underlying technological promise of topological protection, but also positioned it as a promising platform for the fundamental exploration of spinless topological physics. Here, we revisit the question of optimizing photonic bandgaps in this new context of topological PhCs, seeking the automated discovery and optimization of large, topologically nontrivial bandgaps and well-isolated, robust topological degeneracies [4].

The advances in photonic topology have been achieved largely by using analogy, physical intuition, and symmetry requirements. Similarly, optimization of associated designs have depended mainly on parameter sweeps and trial-and-error. Many challenges associated with the highly non-convex and discontinuous optimization space as well as the computational costly evaluation of topology have made it difficult to apply traditional optimization algorithms towards the design of topological PhCs. However, recent theoretical advances have revealed new and powerful insights into the connection between band symmetry, connectivity, and topology [5-7].

In this work, we propose to use a combination of gradient-free optimization algorithms, a symmetry-constrained level-set parameterization of the structure, and a computationally efficient symmetry-based evaluation of band topology to automate the discovery and optimization of novel topological PhCs. An overview of the optimization process' elements is shown in Figure 1. By using a level-set function expressed as a symmetry-constrained Fourier sum, we can parameterize even highly complex geometries using only a low-dimensional parameter space (Figure 1b) which in turn makes both global and local gradient-free optimization algorithms feasible. To efficiently evaluate the band topological constraints, we incorporate the recently introduced frameworks of topological quantum chemistry and symmetry indicators, which have also been applied to PhCs. Furthermore, we use a global optimization algorithm in conjunction with a stochastic local optimization stage to escape local optima during optimization while also handling the non-continuous objective function stemming from the topology of the PhC. We focus on 3D topological PhCs and present novel examples in three settings:

- Γ-enforced topological nodal lines,
- ideal (i.e. frequency-isolated) Weyl points in the interior of the BZ (Figure 2), and
- photonic Chern insulators with chiral surface states.

To our knowledge, these are the first proposed structures with nodal lines and Weyl points in the interior of the BZ, a design task that would be computationally intractable without the use of the symmetry-based topological band analysis tools that we use here. In the last setting, we find a photonic Chern insulator with the largest known complete bandgap, and achieve this without explicitly relying on the supercell modulation technique that underlies earlier designs. While we focus on a handful of concrete topological properties, our method can in principle be applied to any symmetry-identifiable band topology. Requiring no prior examples of topological photonic crystals or prior knowledge on the connection between structure and band topology, our approach indicates a path towards the automated discovery of novel topological photonic crystal designs.

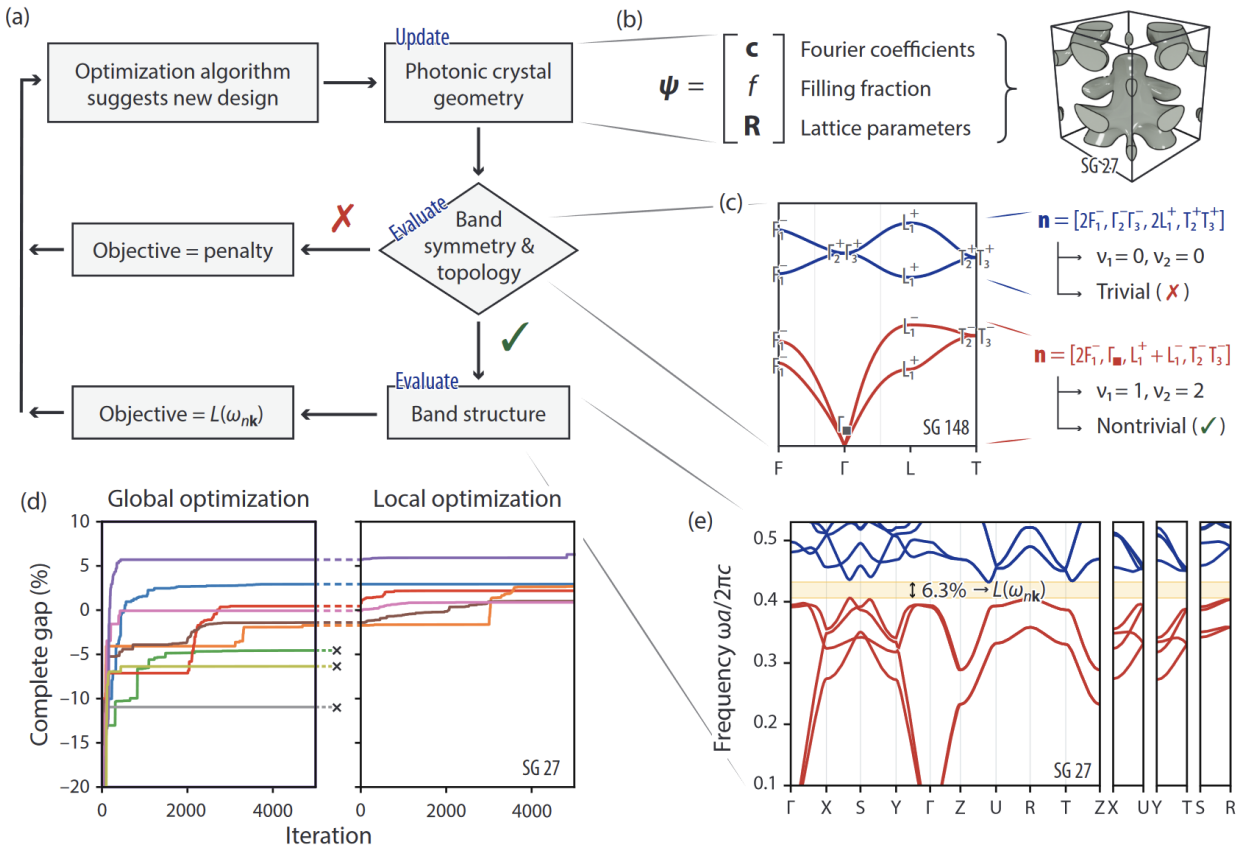

Figure 1. Overview of topological photonic crystal (PhC) optimization. (a) Flowchart of the optimization process in each iteration. (b) The structure of the PhC is parameterized by a continuous vector consisting of the geometry coefficients (the Fourier sum coefficients), the filling fraction, and the unit cell lattice parameters. (c) Symmetry-based tools can be used to calculate the band connectivity and topology from the high-symmetry (HS) k-points, providing a computationally efficient evaluation of the topology constraint (here, exemplified for a hypothetical PhC in space group (SG) 148). (e) If the PhC is found to have the desired topological indicator as computed from the band symmetries, then the bandstructure is calculated along the HS k-lines (shown in purple in the inset). (d) Optimization performance of complete bandgaps in SG 27 over multiple trials, as measured by the best value of the objective found so far as a function of iteration.

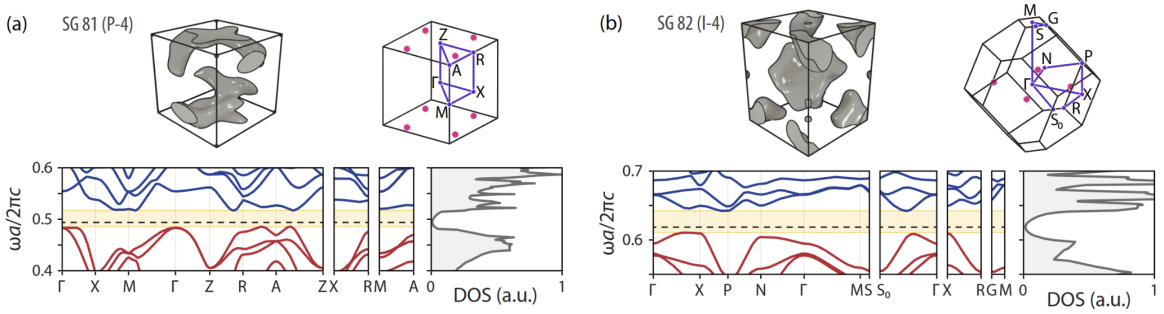

Figure 2. Weyl point optimization in noncentrosymmetric SGs. Selected results for optimized PhCs designs with Weyl points visualized by their dispersions along HS k-lines (red lines, nontrivial valence bands; blue lines, conduction bands; yellow shading, HS gap; dashed black line, Weyl point frequency), density of states (DOS), and Weyl point locations in the B.Z. (a-b) Optimized PhC Weyl point designs in SGs 81 and 82: the unit cells of each design are shown. The BZs feature 4 ideal Weyl points in the $k_z = \pi/c$ plane (with equivalent copies in the $k_z = -\pi/c$ plane) in SG 81 and in the $k_z = 0$ plane in SG 82, without intersecting Fermi pockets. The density of states (DOS) exhibits a parabolic frequency dependence at the Weyl point frequency.

References

[1] L. Lu, J. D. Joannopoulos, and M. Soljačić, Topological photonics, Nat. Photonics 8, 821 (2014).
[2] T. Ozawa, H. M. Price, A. Amo, N. Goldman, M. Hafezi, L. Lu, M. C. Rechtsman, D. Schuster, J. Simon, O. Zilberberg, and I. Carusotto, Topological photonics, Rev. Mod. Phys. 91, 015006 (2019).
[3] G.-J. Tang, X.-T. He, F.-L. Shi, J.-W. Liu, X.-D. Chen, and J.-W. Dong, Topological photonic crystals: Physics, designs, 13 and applications, Laser Photonics Rev. 16, 2100300 (2022)
[4] Kim, S., Christensen, T., Johnson, S. G., & Soljačić, M. (2023). Automated discovery and optimization of 3D topological photonic crystals. *ACS Photonics*, *10*(4), 861-874.
[5] B. Bradlyn, L. Elcoro, J. Cano, M. G. Vergniory, Z. Wang, C. Felser, M. I. Aroyo, and B. A. Bernevig, Topological quantum chemistry, Nature 547, 298 (2017).
[6] H. C. Po, A. Vishwanath, and H. Watanabe, Symmetry-based indicators of band topology in the 230 space groups, Nat. Commun. 8, 50 (2017).
[7] J. Kruthoff, J. de Boer, J. van Wezel, C. L. Kane, and R. J. Slager, Topological classification of crystalline insulators through band structure combinatorics, Phys. Rev. X 7, 041069 (2017).

Location and topology of the fundamental gap in photonic crystals

The pursuit of photonic band gaps has been central to the field of photonic crystals since their earliest inception. Among the most enduring and actively pursued questions is the question of where band gaps can be opened in the band structures of photonic crystals. More recently, significant interest has emerged around the question of which photonic band gaps have nontrivial topological features. Extending recent symmetry-based tools from condensed-matter theory—frequently referred to collectively as topological quantum chemistry or symmetry (TQC)—we pursued these questions, obtaining complete answers to both for the fundamental (i.e., first) photonic gap of three-dimensional photonic crystals.

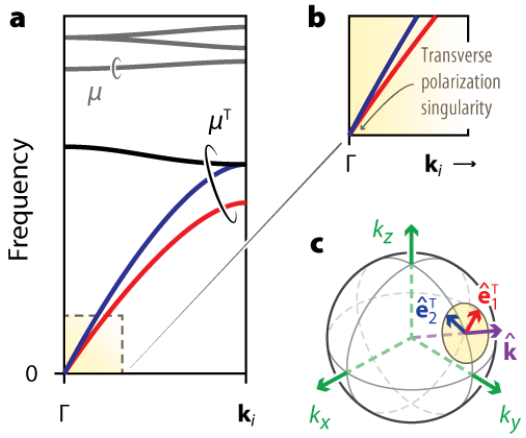

Figure 3. Photonic band connectivity and singularity below the first gap. **a–b** The two lowest-frequency "light-like" photonic bands (blue and red) are pinned to ω = 0 at the Γ-point. The minimum connectivity μ^T of these bands, i.e., below the first gap, is not generally equal to the minimum connectivity μ of higher bands (gray). **c** The polarization vectors $\hat{\mathbf{e}}^{2T}_i$ of the modes near ω = 0 span a space (yellow disk) that depends on the momentum orientation , producing a symmetry singularity at Γ.

The fundamental gap is of special interest because it is typically the most controllable and largest gap in photonic crystals. More interestingly, the fundamental photonic gap is also fundamentally different from all higher-lying gaps because the bands below it feature a unique photonic band singularity at zero frequency (ω = 0) due to the transverse polarization of photons (Figure 3). As a result, the opening of the first photonic band gap is subject to different constraints than all other quasiparticle gaps (e.g., phonons or spinless electrons—but also all higher-lying photonic gaps).

The ability to open gaps depends sensitively on the crystal's symmetry, i.e., its space group, and is constrained by so-called compatibility relations that enforce consistency among band symmetries across the Brillouin zone. By extending TQC to the photonic context and by devising a regularization scheme for the noted singularity, we incorporated these constraints and determined precisely how many bands must exist below the first photonic gap at minimum (Figure 4), answering the fundamental question of where the first photonic gap can be opened. In developing techniques to overcome the noted singularity, we additionally solved the important technical problem of evaluating the first photonic gap's topology using TQC, enabling us to evaluate the symmetry-identifiable topology of *all* minimally-connected fundamental photonic gaps. In doing so, we discovered a new, uniquely photonic topological feature, which we named Γ-enforced topology, associated with photonic topology that is identifiable solely from the number of connected bands below the first gap and is associated with topological nodal lines.

Going forward, we will leverage these advances to pursue high-throughput discovery of photonic topology across all symmetry settings. Additionally, in combination with traditional optimization techniques, we will pursue experimentally fabricable designs of the discovered effect of Γ-enforced photonic topology.

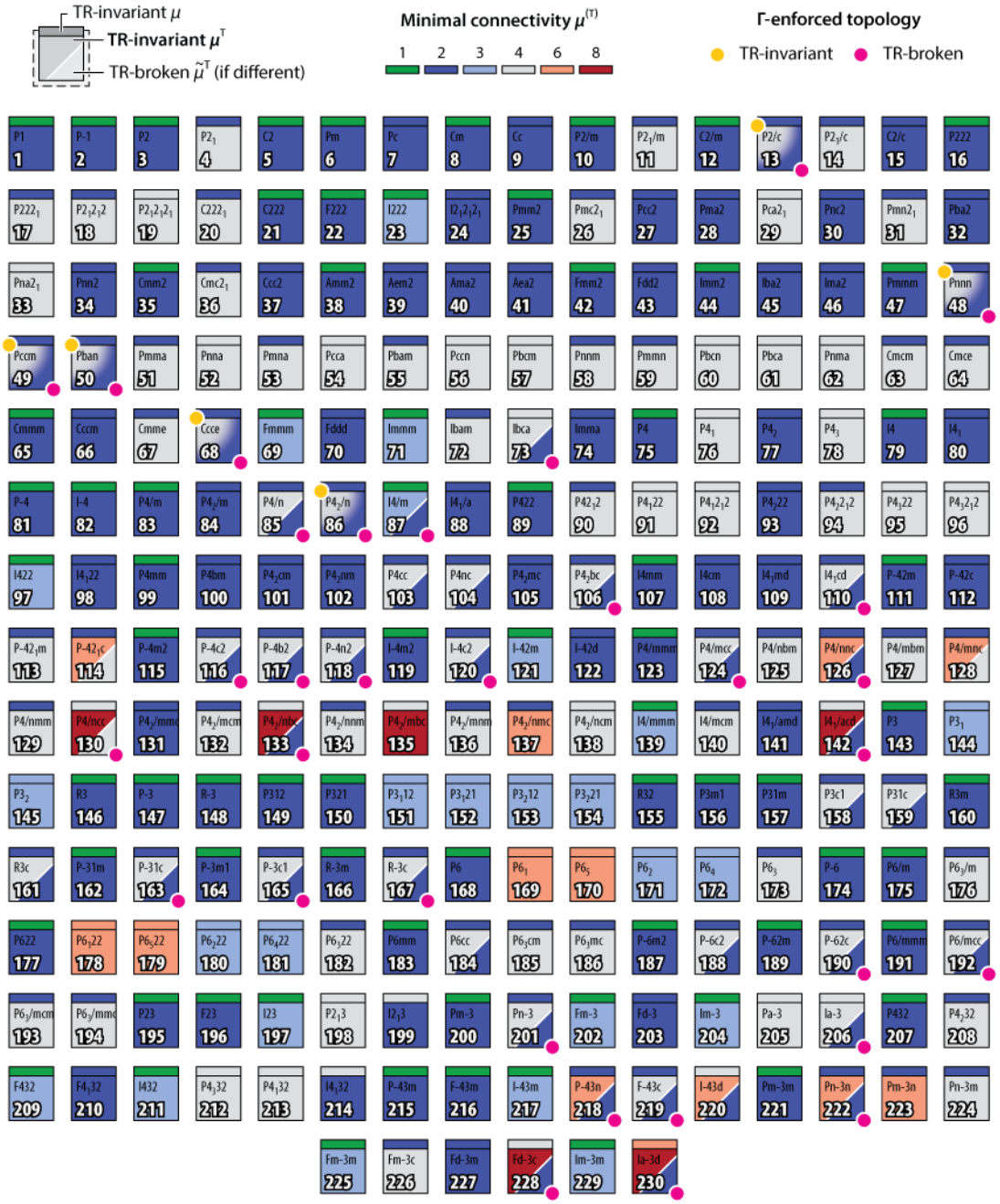

Figure 4. Minimum photonic band connectivity and Γ-enforced topology. The minimum photonic band connectivity below the first gap μ^T for each space group (labeled squares), with time-reversal (TR) symmetry. The corresponding TR-broken connectivities ^{T} are shown (lower triangular

cut-outs) when they differ from μ^T. TR-invariant minimum regular (i.e., associated with all higher-lying gaps) connectivities μ are shown as context (narrow rectangles). Space groups with Γ-enforced topology are highlighted by circular markers.

Generating macroscopic intensity noise-squeezed states of light in semiconductor lasers

The generation of quantum states of light has long been a milestone of quantum optics. An example of such states are squeezed states, in which the uncertainty in one observable (such as photon number or intensity) reduces at the expense of another conjugate observable (such as phase). States of light squeezed in photon number promise numerous applications in quantum information and sensing, allowing, for example, signal detection below the shot noise limit. In the limit of infinite number squeezing, one approaches a so-called Fock state, an energy eigenstate of the electromagnetic field Hamiltonian with a perfectly defined photon number *n*. In addition to their importance as fundamental quantum states of light, Fock states can be used to realize numerous quantum computing protocols that require operations on photon number (e.g., photon number subtraction and boson sampling).

Despite these potential rewards, macroscopic intensity noise-squeezed states of light approaching Fock states are inherently challenging to produce, primarily due to a general lack of nonlinear mechanisms that select specifically for *n* photons, especially where *n* may be large. Moreover, most highly quantum states of light are difficult to maintain, due to the deleterious effects of loss. As such, the state of the art has been limited to few photon Fock states and weakly squeezed states.

To address these issues, we introduced the physical mechanism of nonlinear dispersive loss as a potential new method to create “Fock” lasers, which possess steady state photon number distributions approaching macroscopic Fock states. This phenomenon relies critically on the ability to simultaneously harness strong optical nonlinearities and low background loss (high *Q* cavities). We proposed semiconductor lasers as a potential platform for the Fock laser, owing to their strong nonlinearities, compact form factor, ease of electrical pumping, and wide gain bandwidths. Thus far, noise reduction in semiconductor lasers has been weak and limited primarily to amplitude-phase decorrelation and “quiet pumping” schemes that reduce electrical pump noise.

We have recently shown how semiconductor lasers with a sharp frequency dependent outcoupling could be used to create strongly intensity squeezed light with broadband squeezing of Fano factors 10 dB or more below the shot noise limit. A schematic of our design is shown in Fig. 5, which demonstrates how the combination of sharp dispersive outcoupling and semiconductor optical nonlinearity yields a per-photon loss that depends

sharply and nonlinearly on intracavity photon number. The dispersive outcoupling can easily be provided by photonic crystals fabricated on-chip, low background losses are permitted by high *Q* on-chip resonators, and strong optical nonlinearities are possible using Kerr materials (e.g. GaAs) separate from the active material (e.g. AlGaAs) to avoid resonant effects.

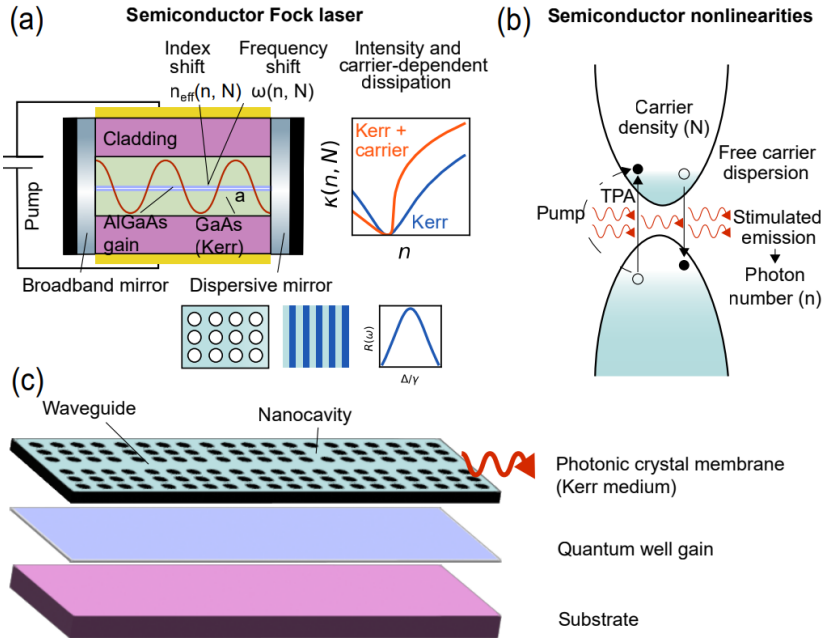

Fig 5: Semiconductor Fock laser architecture with separate gain and Kerr elements. (a) Basic semiconductor laser diode heterostructure design with nonlinear dispersive loss. Dispersive outcoupling is generated via the sharp frequency dependent transmission of a photonic crystal element. Coupling of Kerr nonlinearity from the Kerr material and carrier nonlinearity from the gain material with dispersive loss (frequency dependent reflectivity) creates sharp nonlinear loss κ. Here, Δ denotes detuning from the dispersive resonance and γ denotes the width of the dispersive resonance (related to its FWHM). (b) Semiconductor optical nonlinearities, including intensity dependent Kerr effect as well as carrier-dependent free carrier dispersion (FCD) and two photon absorption (TPA). These nonlinearities shift the real part of the active region's refractive index, in turn shifting the resonance frequency in the diode cavity. Weak nonlinear loss from shifting the imaginary part of the refractive index via the Kramers-Kronig relations is also generated, but in most cases is negligible compared to the nonlinear dispersive loss. (c) Analogous schematic with a photonic crystal (PC) "Fano" laser. The PC platform allows much stronger per-photon nonlinearities due to very small mode volumes. Dispersive loss is provided by waveguide-nanocavity Fano interference in a photonic crystal slab.

Due to the integrated Kerr nonlinearity, as well as free carrier-dependent shifts to the refractive index intrinsic semiconductors, the cavity will have a resonant frequency which depends on the photon number n and inverted carrier density N as $\omega(n,N) = \omega_0(1-\beta n-\sigma N)$, where ω_0 is the bare cavity resonance frequency, β denotes the dimensionless Kerr strength per photon, σ quantifies the strength of free carrier effects and is directly proportional to the linewidth enhancement factor of the active material. When the nonlinear cavity mode is coupled to a dispersive loss, we also obtain a carrier- and intensity-dependent dissipation rate $\kappa(n,N) = -FSR\cdot log[R(\omega(n,N))]$, where FSR is the free spectral range and $R(\omega)$ the frequency-dependent reflection of the resonance.

Such a loss mechanism can have a profound impact on both the steady state and noise properties of the laser. We characterize these properties using a first-principles quantum mechanical approach. We linearize the Heisenberg-Langevin equations of motion for photon and carrier number about their steady state solutions *n, N*. Fourier transforming the linearized equations yields the photon and carrier number noise. The former can be integrated over noise frequency to yield photon number variance $(\Delta n)^2$, from which we calculate the Fano factor $F = (\Delta n)^2/n$, which determines whether the light is above ($F > 1$), at ($F = 1$), or below ($F < 1$) the shot noise limit (squeezed).

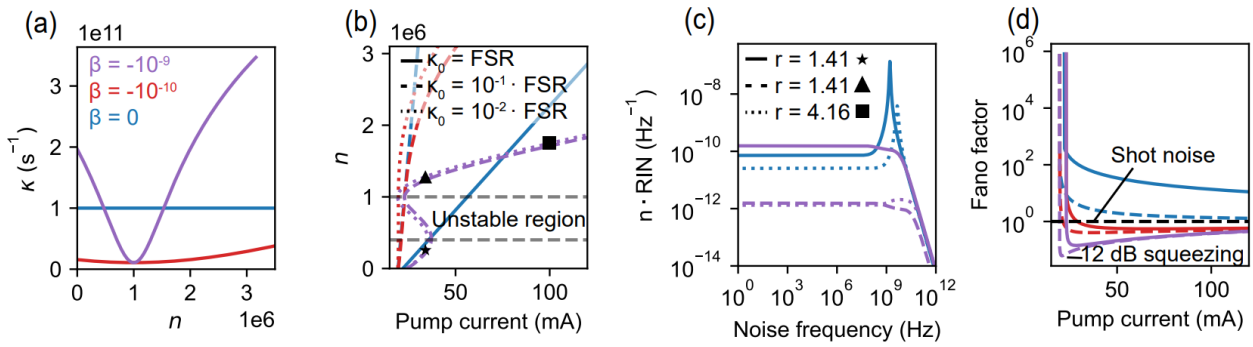

Fig 6: Intensity noise squeezing in semiconductor lasers with dispersive photonic loss and intensity dependent nonlinearity. (a) Intensity dependent loss profiles for three different (dimensionless) nonlinear strengths coupled to symmetric Fano (Lorentzian) dissipation in the absence of carrier nonlinearity. (b) Steady state photon number *n* as a function of pump current (S-curve) for three different linear background losses κ_0 expressed as a fraction of the free spectral range *FSR*. The indicated unstable region is bypassed by the bistable point and is not generally accessible during lasing. (c) Fano factor spectrum as a function of noise frequency for three different pump powers $r = I/I_{thres}$. (d) Fano factor as a function of pump current. Fano factors in (d) are plotted for the low noise (upper) branch in (b) when bistability is present. The Fano resonance decay rate is $\gamma = 2{\cdot}10^{12}$ *rad/s*.

In Fig. 6, we consider a GaAs double heterostructure diode laser with dispersive loss provided by a notch-filter mirror with a Lorentzian reflectivity peak. We consider a modal and active region volume $V = 10^{-16}\ m^3$ bare cavity resonance frequency $\omega_0 = 2.16{\cdot}10^{15}$ *rad/s* (873 nm), and free spectral range *FSR =17 GHz*. Gain parameters and nonlinear coefficients β, σ used are calculated from GaAs experimental data. For weak nonlinearity (red curves), the loss varies weakly with photon number. As photon number increases, so does the loss, decreasing the slope of the input-output curve (S-curve) with increasing pump. For stronger Kerr nonlinearity (purple curves), the loss varies sharply with photon number, with a minimum at $n_c = 10^6$. When the laser is pumped from threshold, the photon number lies below n_c; the loss decreases as the pump and photon number increase, causing the S-curve to steepen and eventually hit a bistable point. The other stable branch is for $n > n_c$, where loss increases sharply with photon number, flattening out the S-curve. It is in this region that the sharp loss exerts a strong feedback on the photon number, reducing the steady state noise level far below the SNL. By operating on the

upper branch (pumping the system past bistability and then lowering the pump), broadband squeezing can be obtained, with Fano factors more than 90% below the shot SNL.

Going forward, we are exploring other dispersive loss mechanisms such as distributed feedback loss and external cavity geometries. We have also simulated noise reduction in quantum cascade lasers and will begin working with experimental collaborators to develop preliminary prototypes in quantum well semiconductor lasers.

Intense squeezed light from lasers with sharply nonlinear gain

In this work, we introduce a mechanism of sharply nonlinear gain which can be used to create intense sub-Poissonian light at optical frequencies. We show how this nonlinear gain can be realized by incorporating Kerr nonlinearity into a traditional solid state laser architecture. We detail how the nonlinear gain acts as a form of “super-saturation,'' leading to new phenomena like nonlinear power curves, and the suppression of transient relaxation oscillations. Furthermore, we show how this nonlinear gain can lead to macroscopic states of light with intensity fluctuations 90% below the shot noise level, which correspond to sub-Poissonian (number-squeezed) states of light that have no classical analog. This is in strong contrast to conventional high-power lasers, which produce coherent states or states with substantial excess intensity noise.

The concept for the “Kerr laser'' is illustrated in Fig. 7a. The system consists of a pumped gain medium in a cavity containing a Kerr nonlinear medium. The Hamiltonian of just a cavity with an embedded Kerr medium (so no gain) is $H_{Kerr}/\hbar = \omega_c a^\dagger a - (\beta/2)(a^\dagger)^2 a^2$. Here, a and $a^\dagger$ are the annihilation and creation operators of the cavity mode, β is the Kerr nonlinear strength of a single photon, and ω_c is the cavity frequency. The cavity resonance frequency depends linearly on the photon number as shown in Fig. 7b. Hence, at a certain Fock state $|n>$ in the cavity, the gain medium and the cavity are resonant (Fig. 7b)

Therefore, the spontaneous emission rate R_{sp} is maximal for photon numbers where the cavity and the gain are resonant, but suppressed for photon numbers where they are detuned. As a result, the cavity “prefers'' photon numbers which are close to resonance, and suppresses photon numbers away from them, leading to a reduction in the photon number fluctuations, and thus squeezing. This type of gain can be thought of as a “super-saturable'' gain, which decreases more sharply with n from the equilibrium point (of balanced gain and loss), as compared to conventional saturable gain. Surprisingly, this approach can lead to very large photon-number squeezing in the cavity (approaching 10 dB), as we will now show.

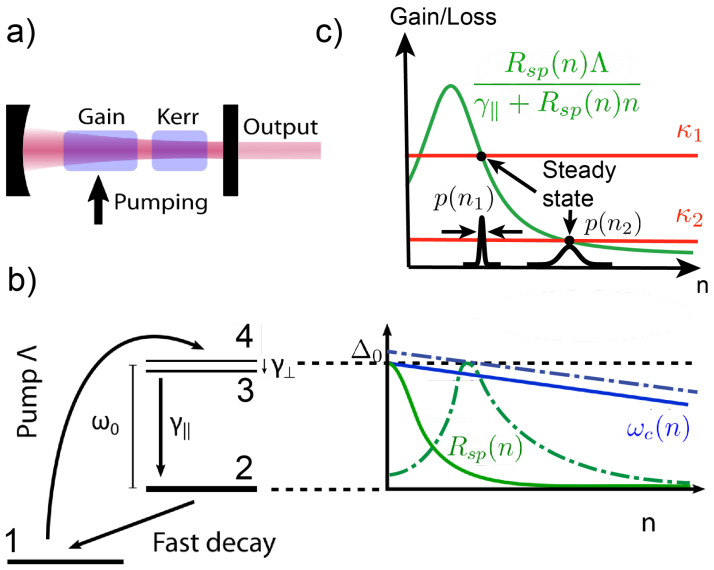

Figure 7: A laser based on Kerr nonlinearity. (a) A pumped gain medium coupled to a cavity with Kerr nonlinearity. (b) Four-level atoms in the gain medium, with lasing transition between level 3 and 2 with frequency ω_0 . The dashed lines show the dependence of the cavity resonance frequency $\omega_c(n)$ (blue) and the spontaneous emission rate R_{sp} (green) on the light intensity of an "off-resonant Kerr laser" ($\omega_c - \omega_0 = \Delta_0$), and the solid lines are those of "resonant Kerr laser." (c) The photon number probability distribution ($p(n_1)$ and $p(n_2)$) depends on the angle between the gain and the loss at their intersection point (or the steady state). Because the gain intersects with the loss κ_1 at intensity n_1 more steeply than with the loss κ_2 at intensity n_2, the probability distribution at n_1 is more squeezed, thus the photon number variance is reduced.

This noise spectrum represents the intensity fluctuations associated with individual Fourier components of the laser field which fluctuates about its steady state. Such fluctuations may be studied with a photodiode and electronic spectrum analyzer. For the linear resonator, the relative intensity noise spectrum sharply peaks around Ω, indicating relaxation oscillations driven by quantum noise. As the nonlinear strength increases, this oscillation peak is suppressed, and eventually eliminated, consistent with the transient behaviors shown for the same parameters (Fig. 8c).

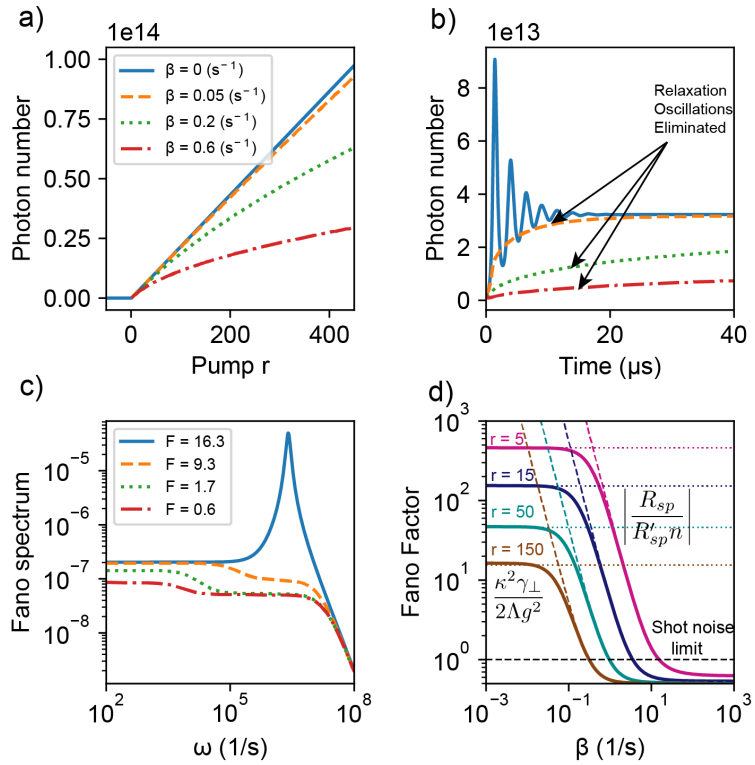

Fig 8: Output characteristics of a "resonant Kerr laser." Parameters used for an Nd:YAG based laser system. For panels (a), (b), and (c) lines with the same color and linestyle have the same β values. (a) Steady-state photon number of a Kerr laser as a function of relative pump rate r for different nonlinear coefficients. (b) Time evolution of photon number at different nonlinear coefficients and at fixed relative pump rate r = 150. (c) The Fano spectrum at different nonlinear coefficients and at fixed relative pump rate t = 150 and their corresponding Fano factors F. (d) Fano factor F at different pump rates as a function of nonlinear coefficient.

Here, we discuss some of the most important considerations relevant to the experimental observation of the effect we proposed. The most important element is that the per-photon nonlinear frequency shift β be as large as possible compared to the polarization decay rate $\gamma_\perp$. This ratio of parameters dictates the effective sharpness with which the gain drops off at higher photon numbers, leading to steady-state intensity noise reduction. Gain mediums Nd:YAG, Nd:YAP and Tm:YAG are all strong candidates due to their relatively narrow gain bandwidths set by $\gamma_\perp$. To maximize the nonlinear interaction β, one should use a material with low absorption and high $\chi^{(3)}$ such as GaP, and consider using a small cavity with a high filling fraction of nonlinear material so that the intensity-dependent frequency shift is as large as possible. Note that while in principle, some of these materials (e.g., GaP) have two-photon absorption, it is quite weak, and may not be detrimental as such effects can lead to further number squeezing. If two-photon

absorption is not desired, then one can use a gain medium such as Er:YAG, Tm:YAG, or Tm:YAP, which have lasing wavelengths below the two-photon absorption cutoffs of Kerr materials such as GaAs and GaP. It is also worth pointing out that stronger Kerr shifts can be achieved at higher intensities. Thus, it is desirable to design a laser cavity that has highly reflective mirrors so that the intracavity power is orders of magnitude higher than the outcoupled power. The cavity parameters used in this work are consistent with those which can be realized experimentally.

While for the sake of concreteness, we have based our discussions around a well-established solid-state laser geometry using a free space optical cavity, the concepts developed here should readily extend to other laser platforms, so long as the gain medium has a low bandwidth, and an appropriate amount of Kerr nonlinearity. Additional candidates for narrow bandwidth gain media could include gasses, engineered semiconductor, or quantum well transitions. On-chip platforms have the additional advantage that nanophotonic techniques can be used to engineer small mode volumes and efficient Kerr nonlinearity.

In summary, we have proposed a laser architecture that uses sharply nonlinear gain to generate macroscopic sub-Poissonian light. We have discussed how this architecture can be implemented at optical frequencies using conventional solid state gain materials in conjunction with Kerr nonlinear materials. The parameters we have considered are experimentally accessible, and can lead to intra-cavity light which is 90% below the shot noise limit. Importantly, the minimum achievable noise reduction is set purely by the parameters of the implementation (as opposed to mechanisms such as two-photon absorption, which have an intrinsic squeezing limit). Thus, with further optimization of the gain lineshape and Kerr nonlinearity on potentially different platforms, it may be possible to go far below the 10 dB reduction we discussed here, eventually leading to the generation of macroscopic near-Fock states. More broadly, this work points toward the further investigation of novel optical nonlinearities as a means to create quantum states of light.

Optical properties of dispersive time-dependent materials

Time-varying optical materials have attracted recent interest for their potential to enable frequency conversion, nonreciprocal physics, photonic time-crystals, and more. However, the description of time-varying materials has been primarily limited to regimes where material resonances (i.e., dispersion) can be neglected. In this work, we describe how the optics of these dispersive time-varying materials emerges from microscopic quantum mechanical models of time-driven systems. Our results are based on a framework for describing the optics of dispersive time-varying materials through quantum mechanical linear response theory. Importantly, we clarify how response functions for time-varying materials are connected to energy transfer. We provide three examples of our framework

applied to systems which can be used to model a wide variety of experiments: few level models that can describe atoms, spins, or superconducting qubits, oscillator models which can describe the strong response of polar insulators, and strongly driven atom models which can describe the highly nonperturbative optical response of materials undergoing high harmonic generation. We anticipate that our results will be broadly applicable to electromagnetic phenomena in strongly time-varying systems.

Many of the basic assumptions about the nature of optical response and wave propagation rely on considering optical materials as time translation-invariant --- the same at all times. However, a recent surge of interest has developed in the possibilities that may be enabled by materials which break this assumption --- in other words, materials which vary in time. In practice, time-varying materials are typically created by applying strong temporal modulations to stationary materials in the form of external fields. These time-varying materials may exhibit rich physics such as frequency conversion, scattering from temporal interfaces, nonreciprocity, and amplification. Moreover, a recent interest has sparked in the study of so-called “photonic time crystals'' which have a strong temporally periodic index variation, enabling new directions in topological physics and light-matter interactions. Additionally, the possibility of strongly time-modulated materials introduces new fundamental questions about the nature of quantum light-matter interactions in time-modulated systems, including control over the generation of entangled photon pairs.

In this work, we present a general framework which describes the optics of dispersive time-dependent materials based on microscopic quantum mechanical dynamics. By doing so, we answer a fundamental question about the nature of energy transfer in time-varying systems, namely the significance (or in some cases, lack thereof) of the imaginary part of response functions. We also specialize many of our results to the particularly intriguing case of time-periodic (i.e. “Floquet'') systems. In this case, many of our results are simplified by the use of Floquet theory to describe both the quantum and macroscopic electromagnetic aspects of problems. We provide examples of our framework across a variety of systems: time-modulated superconducting qubits in the GHz, time-modulated polar insulators with optical phonon resonances, and strongly driven gasses which exhibit high harmonic generation (HHG). Our framework, when applied to these systems, enables us to discover a wide range of physics such as pulse propagation in dispersive photonic time-crystals, nonperturbative frequency conversion, and energy loss/gain.

We briefly describe our general framework for constructing new time-dependent optical materials from microscopic quantum mechanical models (Fig. 9). In such models, the dynamics are described by the solution to the Schrodinger equation with a time-dependent Hamiltonian H(t). Generally, these microscopic dynamics can depend on many-body effects in a complicated manner. In this work, we will focus on materials which are well-described by constructing an effective bulk response from a collection of single particle dynamics; however, many of our conclusions hold more broadly. Once the

relevant Schrodinger equation has been solved, the dipole response functions of single particles can be constructed, and then transformed into bulk macroscopic response functions such as $\varepsilon(\omega, \omega')$. In systems where dissipation mechanisms are important, this process can also be followed by solving an appropriate master equation which rigorously incorporates the dissipative dynamics.

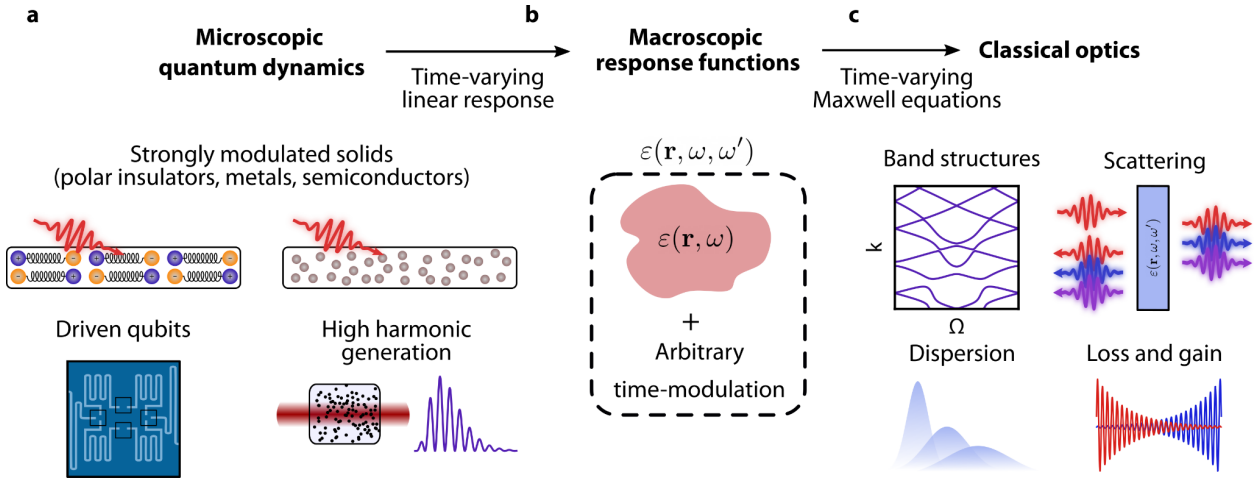

Figure 9: General framework for describing the optics of dispersive and strongly time-dependent systems. (a) Examples of time-dependent quantum mechanical systems whose optical response requires time-varying linear response theory. (b) Models of these microscopic dynamics can then be used to construct macroscopic response functions which may also vary spatially to account for material structures. For example, a dispersive dielectric structure $\varepsilon(r, \omega)$ in the absence of time-modulation can be described in terms of a two-frequency response function $\varepsilon(r, \omega, \omega')$ in the presence of time-modulation. (c) These response functions can be incorporated into the Maxwell equations to describe optical features of these systems, such as “free'' wave propagation, scattering, and energy transfer.

With a macroscopic response function in hand, one can then use classical electrodynamics to describe wave propagation and energy transfer in dispersive time-varying media. For example, strongly modulated systems which are periodic in time (photonic “time crystals'') can be associated with a band structure which indicates the relationship between wavevector and quasi-frequency in the driven material (see dispersion diagram in Fig. 9c). In systems with strong light-matter hybridization, this provides a direct way to solve for the polaritons of the driven system. Another example is the use of time-dependent response functions to compute frequency-dependent scattering from a structure such as a thin film of a time-dependent material.

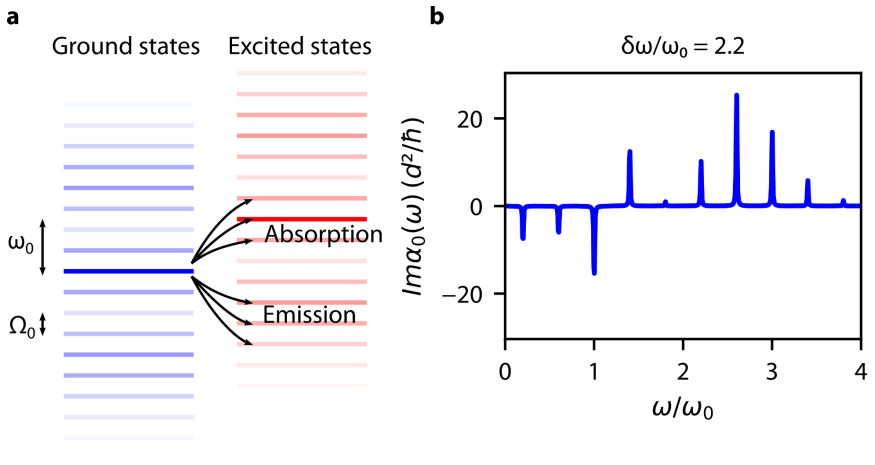

Figure 10: Linear response representation of ground state gain in a driven two-level system. (a) Floquet level diagram for a two-level system driven at frequency $\Omega/\Omega_0 = 0.4$ with strength $\delta\omega/\omega_0 = 0.2$. Arrows indicate absorptive and emissive transitions from the thermodynamic ground state to the excited state. (b) Energy transfer properties of the driven system can be visualized through $Im\,\alpha_0(\omega)$. Transitions with loss correspond to peaks where $Im\,\alpha_0(\omega) > 0$, while transitions with gain correspond to peaks where $Im\,\alpha_0(\omega) < 0$.

One question of key importance in strongly time driven systems is the way in which an external probe field exchanges energy with the system. In particular, systems which are independent of time, and in equilibrium, can only exhibit passive absorption, and cannot exhibit any gain. However, strongly driven systems no longer satisfy this property. One of our main accomplishments in this piece of work was to provide clarity on the relationship between the response functions of time varying systems, and the energy loss or gain in the system.

Our findings are summarized as follows: A response function such as $\alpha(\omega, \omega')$ contains both real and imaginary parts. The part part of this function for which $\omega = \omega'$ does encode absolute significance about energy transfer. In particular, the real and imaginary parts of the "diagonal" part of the response function give the reactive and absorptive contributions, respectively. However, in general, the rest of the function ($\omega \neq \omega'$), does not have this absolute significance. These contributions can give either gain or loss depending on the phase of the probe.

We give an example of the resonant gain and loss that can be achieved in a time modulated two level system. To do so, we consider a modulated two-level system with $\Omega = 0.4\omega_0$. When strongly modulated, a substantial contribution emerges from Floquet sidebands which fall below the level of the original ground state. This means that the system can make ground to excited state transitions at frequencies $\omega_0 + k\Omega_0 < 0$ for

sufficiently negative integers k. These transitions are schematically shown in Fig. 10a. In the polarizability, these transitions appear as peaks with $Im\,\alpha_0(\omega) < 0$ around the relevant resonances, corresponding to energy gain in the Floquet ground state. The gain peaks appear next to other peaks where $Im\,\alpha_0(\omega) > 0$, which correspond to absorptive transitions. Thus, a two-level system modulated in this way can provide either absorption or gain to a probe field, depending on the frequency.

One important future direction is the development of microscopic models to describe time-varying linear response in more complex systems. For example, many recent works have focused on the electronic states that can be created in Floquet-driven matter (with a particular focus on topological electronic properties). However, there is still much work to be done to use these descriptions of strongly driven solids to infer the optical properties of such materials. In some cases, free electron or few-band models may be sufficient to capture the key physics. In more complicated situations, time-dependent density functional theory (TDDFT) may serve as an essential tool for computing time-varying response functions (for example, $\varepsilon(\omega, \omega')$ for a strongly driven semiconductor). Once the optical response of a strongly driven material is appropriately characterized, it can be incorporated into either classical or quantum descriptions of electromagnetic phenomena.

It will also be critical to develop methods for characterizing general time-varying optical response through pump-probe experiments. Many experimental platforms of current study consist of planar structures (polar insulators or ENZ materials) which are strongly driven. A typical protocol should consist of fixing the pump conditions, and then measuring the amplitude and phase change of a probe which is varied in amplitude and phase. Such a measurement of complex reflection or transmission carries information which in many cases can be used to infer the material response functions based on a model of the geometry. We anticipate that this framework will become essential for describing the optical response of a wide variety of systems, as described.

Annual Report for Grant FA9550-20-1-0115 (Sept 2023)
Topological photonics for enabling high-power lasers

Published content:

Publications

1. Christensen, T., Po, H. C., Joannopoulos, J. D., & Soljačić, M. (2022). Location and topology of the fundamental gap in photonic crystals. *Physical Review X*, *12*(2), 021066.

2. Kim, S., Christensen, T., Johnson, S. G., & Soljačić, M. (2023). Automated discovery and optimization of 3D topological photonic crystals. *ACS Photonics*, *10*(4), 861-874.

3. Roques-Carmes, C., Kooi, S. E., Yang, Y., Rivera, N., Keathley, P. D., Joannopoulos, J. D., ... & Soljačić, M. (2023). Free-electron–light interactions in nanophotonics. *Applied Physics Reviews*, *10*(1).

4. Rivera, N., Sloan, J., Salamin, Y., Joannopoulos, J. D., & Soljačić, M. (2023). Creating large Fock states and massively squeezed states in optics using systems with nonlinear bound states in the continuum. *Proceedings of the National Academy of Sciences*, *120*(9), e2219208120.

5. Yang, Y., Roques-Carmes, C., Kooi, S. E., Tang, H., Beroz, J., Mazur, E., ... & Soljačić, M. (2023). Photonic flatband resonances for free-electron radiation. *Nature*, *613*(7942), 42-47.

6. Ma, A., Zhang, Y., Christensen, T., Po, H. C., Jing, L., Fu, L., & Soljačić, M. (2023). Topogivity: A machine-learned chemical rule for discovering topological materials. *Nano Letters*, *23*(3), 772-778.

7. Yang, Y., Po, H. C., Liu, V., Joannopoulos, J. D., Fu, L., & Soljačić, M. (2022). Non-Abelian nonsymmorphic chiral symmetries. *Physical Review B*, *106*(16), L161108.

Preprints

1. Sloan, J., Rivera, N., Joannopoulos, J. D., & Soljačić, M. (2022). Optical properties of dispersive time-dependent materials. *arXiv:2211.16166*.

2. Nguyen, L., Sloan, J., Rivera, N., & Soljačić, M. (2023). Intense squeezed light from lasers with sharply nonlinear gain at optical frequencies. *arXiv:2306.01908*.

3. Pontula, S., Sloan, J., Rivera, N., & Soljačić, M. (2022). Strong intensity noise condensation using nonlinear dispersive loss in semiconductor lasers. *arXiv:2212.07300*.

Annual Report for Grant FA9550-20-1-0115 (Sept 2023)
Topological photonics for enabling high-power lasers

Conference Presentations

1. Pontula, S., Sloan, J., Rivera, N., & Soljačić, M. (2023, May). Strong quantum mechanical squeezing based on nonlinear dispersive loss in semiconductor lasers. In *CLEO: Science and Innovations* (pp. SF3L-6). Optica Publishing Group.

2. Sloan, J., Gorlach, A., Tzur, M. E., Rivera, N., Kaminer, I., & Soljačić, M. (2023, May). Entangling X-rays through high harmonic down conversion. In *CLEO: Fundamental Science* (pp. FW4M-1). Optica Publishing Group.

Patents